Surface energy driven agglomeration and growth of single crystal metal wires

Journal:	*Nano Letters*
Manuscript ID:	nl-2010-04357e.R1
Manuscript Type:	Communication
Date Submitted by the Author:	02-Feb-2011
Complete List of Authors:	Jung, Soon Jung; Trinity College Dublin, Chemistry Lutz, Tarek; Trinity College Dublin, Physics Boese, Markus; Trinity College Dublin, Center for Research on Adaptive Nanostructures and Nanodevices (CRANN) Holmes, Justin; University College Cork, Department of Chemistry Boland, John; CRANN Trinity College Dublin, Chemistry

Surface energy driven agglomeration and growth of single crystal metal wires

Soon Jung Jung[1, 3], *Tarek Lutz*[2,3], *Markus Boese*[3], *Justin D. Holmes*[3, 4] *and John J. Boland** [1, 3]

[1] School of Chemistry, Trinity College Dublin, Dublin 2, Ireland.

[2] School of Physics, Trinity College Dublin, Dublin 2, Ireland.

[3] Center for Research on Adaptive Nanostructures and Nanodevices (CRANN), Trinity College Dublin, Dublin 2, Ireland.

[4] Materials and Supercritical Fluids Group, Department of Chemistry and the Tyndall National Institute, University College Cork, Cork, Ireland

AUTHOR EMAIL ADDRESS jboland@tcd.ie

RECEIVED DATE (to be automatically inserted after your manuscript is accepted if required according to the journal that you are submitting your paper to)

CORRESPONDING AUTHOR FOOTNOTE .

Name: John J. Boland

Telephone: +353 1 896 3140

Fax : +353 1 896 3142

email address: jboland@tcd.ie

Keywords: Au nanowire, Cu nano wire, surface energy, agglomeration, eutetic

ABSTRACT

We introduce a novel wire growth technique that involves simply heating a multilayer film specifically designed to take advantage of the different surface energies of the substrate and film components. In all cases the high surface energy component is extruded as a single crystal nanowire. Moreover we demonstrate that patterning the bilayer film generates localized surface agglomeration waves during the anneal that can be exploited to position the grown wires. Examples of Au and Cu nanowire growth are presented and the generalization of this method to other systems is discussed.

KEYWORDS.

Growth method, Single crystal, Au wire, Cu wire, Surface energy, Agglomeration

MANUSCRIPT TEXT

Metal alloys with eutectic compositions are key enabling materials in nanotechnology. The pioneering studies of Wagner and Ellis[1] showed that $SiCl_4$ decomposition on Au results in the formation of eutectic Au-Si droplets, which become supersaturated and ultimately lead to the growth of Si whiskers whose diameters are controlled by the droplet size. Lieber *et al* [2] subsequently demonstrated pulsed laser ablation of a $Si_{0.9}Fe_{0.1}$ target and following which nanowire materials became more widely available. Since then numerous methods have been developed to control the melting of metal films and/or the creation and positioning of nanoparticles as nuclei for materials growth.[3-5] There are now facile routes for materials synthesis enabled by the formation and manipulation of the properties of eutectics,[2-17] Prior studies have focused almost exclusively on the formation of a high purity non-metal component that is driven by the continuous decomposition of growth precursors delivered via gas or liquid phase reaction. Here, we report on a previously unobserved phenomenon in which a eutectic droplet created by simply

heating a multilayer film can be driven to form single crystalline whiskers or nanowires of the metallic phase. Using cross section analysis of individual eutectic droplets we demonstrate that this is due to a surface energy driven phenomenon that forces the high surface energy material of a multilayer film to be extruded from the eutectic droplet in the form of a single crystalline wire. Moreover, we demonstrate that it is possible to control the surface diffusion and agglomeration by patterning the bilayer film to generate localized surface agglomeration waves, which can be exploited to control the position the grown wires.

Multilayer samples were fabricated using Si(100) substrates (2 inch diameter, 275±25 µm thick, N-type As-doped wafer, purchased from Semiconductor Wafer, Inc.) containing a 30-40 nm thermal oxide layer. Different thicknesses of polycrystalline Au and amorphous Ge films[18] were deposited by varying the sputter-deposition time using a magnetron sputter-coater (208 HR) and monitored by quartz crystal microbalance. Multilayer samples were annealed for typically 12 hours at 400 °C (see below) in the 10:90 atmosphere of hydrogen and argon at a flow rate of 60 sccm and reaction pressure of 350 mTorr, with heating and cooling rates of 100 °C / hour. These conditions were chosen because the Au-Ge eutectic comprised of 27.0 at. % Ge melts at 356 °C.[19] All characterisations were performed after the sample had cooled to room temperature. The surface morphology, crystal structure, and composition were characterized by scanning electron microscopy (SEM, Carl Zeiss, Ultra), energy dispersive analysis (EDX, Carl Zeiss, Ultra) and transmission electron microscopy (TEM, FEI Titan).

The phase diagram of Au-Ge has deep eutectic at 361 °C and 28.0 at. % Ge, respectively. [19] At this composition, the material can be melted and recrystallized even though this temperature is much lower than the melting points of the pure components, 1064 °C for Au and 938 °C for Ge. The low temperature recrystallization of amorphous semiconductors in the presence of a metal is well known and termed metal-enhanced crystallization.[20,21] Here, we focus on the crystallization and growth of metals

when in contact with a semiconductor.

Au-Ge bilayers were prepared on the Si(100) substrate by sputter or thermal deposition. The Si(100) surface has a 40 nm oxide layer and the Au/Ge bilayer consist of amorphorous Ge and polycrystalline Au prior to annealing the deposited films.[18] When only a 10 nm Ge layer is deposited on Si(100) the sample is unchanged after 12 hours annealing at 400 °C (Fig. 1(a)). Following the incorporation of just 1 nm of Au between the Ge layer and Si(100) substrate, the system melts and recrystallizes. The sample was heated to above the eutectic temperature, resulting in formation of eutectic liquid that opens up diffusion pathways for Au and Ge atoms. The SEM image in Fig. 1(b) shows Ge flakes between Au clusters (see Supplementary Information). The surface energy of Au (1.33 J/m^2) is higher than the surface energy of liquid Ge (1.00 J/m^2), so that the Au tends to de-wet with higher curvature than Ge on the SiO_2 surface resulting in Au cluster formation.[22] After further increasing the amount of Au to form a Au 5 nm / Ge 10 nm bilayer, Fig. 1(c) shows that after the 400 °C anneal the surface becomes disordered and comprised of connected clusters of Au particles. This fractal structure is similar to the well known diffusion-limited aggregation (DLA) structure first identified by Witten and Sander.[23,24] Within the DLA model Au atoms progressively diffuse through the Au/Ge eutectic liquid layers until they become attached to larger Au particles, ultimately leading to the formation of the diffusive dendrite-shaped Au networks seen Fig. 1(c).[25,26] However, in our system, in addition to the DLA model, we demonstrate the Au atom undergo crystal formation instead of the more usual “aggregation”. In particular, when we increased the bilayer composition to Au 10 nm/Ge 10 nm, the fractal-like structures disappeared and previously unreported ball-like droplets and Au crystallites are observed (see below). A first clue comes from the contrast changes observed on the Si substrate in Fig. 1((c) and (d)). The bright dendrite-shaped Au areas in Fig. 1(c) are replaced by similarly-shaped but darker Si areas in Fig. 1d that terminate at the ball-like droplets. Clearly, the effect of increasing the Au layer thickness from 0 nm in Fig. 1(a) to 10 nm in Fig. 1(d), enhances Au diffusion facilitating the growth of ball-shaped droplets and ultimately Au crystallites (see below). In addition, the surface is heterogeneous such that droplets in

different regions have access to different supplies of Au which in turn controls the extent of the structural transformation.

We have analyzed over one hundred different droplets, and identified a structural transformation that correlates with the growth of single crystal Au whiskers and nanowires. Enlarged images of representative clusters are shown in Fig. 1(e)-(m). In Fig. 1(e) the ball shape cluster exhibits a eutectic microstructure on its surface (see the supplementary information). The pattern reflects the separation of the Ge and Au components that occurs after solidification and cooling, and is commonly observed after quenching eutectic mixtures.[27] Fig. 1(f) however shows a ball shaped droplet where there is a distinct patch on the surface from which the expected eutectic microstructure is absent (yellow arrow). This area becomes larger in Fig. 1(g) and in Fig. 1(h) a hexagonal shaped feature begins to emerge from the middle of the ball. Figure 1(i)-(j) show the further progression of this growth that ultimately results in the formation of a truncated octahedron structure bounded by {111} facets, the densely packed and hence the energetically most favorable surface for face centered cubic (fcc) materials. This shape evolution is consistent with similar observations during the growth Au nano-particles.[13,28,29] EDX mapping of these ball shaped structures (see Supplementary Information), confirmed that the eutectic microstructure regions (in Fig. 1(e)) are comprised of Au and Ge, while those areas that do not contain eutectic microstructure are comprised exclusively of Au. Fig 1(k)-(m) show the final growth phase that results in the formation of perfect single crystal Au wire (see below).

Fig. 2(a) shows a droplet that exhibits large regions of non-eutectic microstructure on its surface. To explore the growth phenomenon a section from this Au-Ge eutectic ball was cut (white box in Fig. 2(a)) out using focused ion beam (FIB). After FIB polishing a cross-sectional lamellar was generated (Fig. 2(b)) to allow structural studies using transmission electron microscopy (TEM). The FIB-cut cross section in Fig. 2(b) reveals the droplet contains a hexagonal structure that has phase separated from the

remainder of eutectic alloy. The high resolution transmission electron microscopy (HRTEM) image in Fig. 2(c) and the electron diffraction image of this area in Fig. 2(d) confirm the hexagonal structure is a single crystal of Au with the bulk lattice spacing along the [110] zone axis. The top surface of the Au crystal in the droplet is identified as a {111} surface by HRTEM and the diffraction pattern deduced from the [110] zone axis. We note that orientation of the Au crystal is not influenced by the Si substrate since the thermal oxide layer on the Si surface is stable at 400 °C,[30] but instead is driven by the lowest energy facets for bulk Au. EDX shows no detectable level of Ge within the Au single crystal but identifies the presence of a thin layer of pure amorphous Ge surrounding the entire crystal (see arrows in Fig. 2(b)).

Increasing levels of Au diffusion and supersaturation ultimately lead to the growth of Au whiskers and nanowires from the Au seeds contained within the droplets (Fig. 2). The longest wire grown from the Au 10 nm/Ge 10 nm bilayer film was ~ 75 μm long (Fig. 3(a)). To analyze the structure we choose a large Au wire for TEM analysis since it was easy to pluck from the Si(100) substrate and transfer it to a TEM grid using a micromanipulator. FIB thinning was required, since the 4 μm diameter wire was too thick for TEM analysis (inset Fig. 3(a)). Within the better than 1 at.% detection sensitivity of EDX for Ge, the wire is comprised entirely of Au, while the root ball region shows measurable levels of Ge (Fig. 3(b)). The HRTEM image of a selected region in Fig. 3(c) shows clearly resolved lattice planes of single crystal Au structure. The corresponding fast Fourier transform (FFT) of the HRTEM image (inset of Fig. 3(c)) shows the diffraction pattern from the Au structure with a [1 1 0] zone axis, indicating the wire grows along the (1-11) direction. We randomly checked several sites along the wire and confirmed that it is a single crystal through its entire length with same crystal orientation.

The droplet structure and wire growth phenomenon can be understood in terms of the Au-Ge phase

diagram[19] in Fig. 4 and the enhanced diffusion of Au over that of Ge.[31-33] On heating to 400 °C the Au/Ge bilayer melts to form a eutectic alloy containing 24.5 to 29.5 at. % Ge (I in Fig. 4). Sa *et al.* calculated the compositional dependence of the surface energy (γ) of Ge-Au alloys.[22] For binary alloys containing Ge (γ = 0.77 J/m^2) and Au (γ = 1.33 J/m^2) at 400 °C, the surface energy decreases with increasing Ge content, and the surface energy of a eutectic alloy that contains 24.5 - 29.5 at. % of Ge is expected to be 1.05 - 1.15 J/m^2. Consequentially, the Au-Ge bilayer on top of SiO_2 layer (γ = 0.75 J/m^2) is morphologically unstable and the alloy tends to de-wet and form a droplet at 400 °C.[22] During the 12 hours anneal, the eutectic droplet increases in size due to the dissolution of additional Au and Ge by surface diffusion. Under these conditions the droplet cannot maintain the equilibrium composition since the diffusion rate of Au is much faster than Ge.[31-33] As the size of eutectic ball increases, the composition shifts to the Au supersaturated region following the tie line drawn at 400 °C (II in Fig. 4). Due to the lower surface energy of liquid Ge (γ = 0.77 J/m^2) compared to liquid Au (γ = 1.33 J/m^2) at 400 °C,[22] the surface of the liquid eutectic ball becomes Ge enriched. Hgher levels of Au supersaturation result in the formation of a solid Au crystal in the center region of the droplet surrounded by a Ge-rich composition, resulting in the formation of a cored droplet structure (Fig. 2). Additional incorporation of Au leads to further growth of the of Au crystallite and ultimately the formation of an Au wire (Fig. 3). We suggest that this behavior is a consequence of the capillary or Gibbs-Thomson pressure associated with growth from a high curvature surface.[7] Holmberg et al. directly visualized just such a capillary effect in which an Au particle was pushed up from spherical tip of a carbon shell nano-cylinder into the stem of a growing Ge nanowire.[9]

As cooling begins, the composition of the liquid surrounding the Au crystal will change until the eutectic temperature is reached. As the temperature continues to fall to just below the eutectic temperature, the liquid phase, which has the eutectic composition, transforms into the characteristic

eutectic solid structure, i.e., alternating Au and Ge lamellar structure. After rapidly quenching the sample following a 12 hour anneal, Au wires were still observed, indicating the growth occurs at elevated temperature and is not an artifact of the cooling process. Moreover, by increasing the annealing time from 1 hour to 12 hours, the number density and the length of the wires are significantly increased indicating that material diffusion and agglomeration is the rate limiting step for wire growth.

It is important to point out that despite the larger thermal expansion coefficient of Au relative to Ge [34-37] the present wire growth mechanism is not related to the widely reported stress induced whisker growth on the surface of metals, such as Zn, Cd, Bi and Sn.[38-42] In the case of the latter when a highly compressive stress is present in a thin film comprised of a low melting point and a high melting point material, the low melting point material is extruded from the surface in the form of wire, provided the temperature is sufficiently high for the low melting point material to diffuse.[43] This contrasts with the present growth mechanism in which the high melting point material is grown (Au in this case), and which is surrounded by a liquid eutectic under growth conditions and hence unable to exert a compressive stress on the Au crystal. Moreover, the present growth is different from standard VLS growth since the eutectic ball is at the wire bottom, in contrast to the latter where the ball is found at the top of the wire (see Supplementary Information).

Given the model proposed here, wire growth should be possible in a wide range of material systems. The requirements are a substrate with low surface energy, a catalyst material of intermediate surface energy (Ge in the present example) and a higher surface energy growth material (Au). The success of the method depends on the latter materials being able to readily intermix and agglomerate under the growth conditions. The Ge-Cu binary system has a eutectic temperature of 644 °C.[44] Once again we find the high surface energy Cu component (γ = 1.8 J/m^2)[45] segregates out as single crystalline nanowires that under the present conditions have diameters that range in size from 30 to 100 nm (see Supplementary Information). The present focus on the Au-Ge system is that the droplets are large, easy

to handle and analyze and hence easier to investigate the growth mechanism. The growth method, however, is not limited to binary systems or to the growth of the metal component. In many situations it may be advantageous to consider ternary or more complex multilayer systems, where the addition of a new component selected based on surface energy and miscibility, facilitates intermixing and enables processing under more favorable conditions, lower growth temperature or shorter growth times.

Finally, we now show that it is possible to control the atomic diffusion and aggregation dynamics so as to control the placement of single crystalline wires. Fig. 5(a) shows the growth of Au wires on a 10 nm Au/10 nm thick Ge film that is patterned so as to leave exposed region of the low surface energy Si (100) substrate. The dramatic increase in the number density of wires is due to enhanced agglomeration caused by the well known edge effect at the film boundary where the substrate is exposed .[46] The diameter and length distributions of the wires in Fig. 5(a) are shown in the supporting information. The Au/Ge layer is unstable and tends to contract and form a rounded shape that minimize the surface energy, and which through the mechanism detailed above ultimately leads to Au wire growth inside the original Au-Ge patterned area. Placing holes (200 nm diameter and 50 nm deep) within this patterned layer creates an array of local sites for enhanced agglomeration. Effectively, the hole acts as a preexisting critical void that initiate the diffusion mechanism.[46] This results in the circular wavefronts of materials that spreads outwards from each site during the annealing process (Fig. 5(b)). This behavior is consistent with a de-wetting agglomeration model in which voids, defects in the film and the films edges, are nucleation sites due to the presence of exposed regions of the lower energy substrate.[46,47] By appropriately positioning holes it is possible to cause these diffusion wavefronts to interfere, creating a spatially organized pattern of material (Fig. 5(c) and (d)). To demonstrate this phenomenon, we designed a regular hole array having two different pitches (α and β in Fig. 5(f)). The wavefronts propagates away from these holes and material accumulates at the interference positions, resulting in the array of the single crystal Au wire shown in Fig. 5(f). Whilst the wire array is far from perfect it does indicate an ability to position materials and wires by exploiting surface agglomeration waves. We also

note that the wires in Fig. 3 and 5 are qualitatively different. This is visually demonstrated in Fig. 5(e), which shows Au nanowire (~ 300 nm in diameter) with well developed facets that clearly follow the bulk crystallography even as the wire changes growth directions. The former was grown via random diffusion into a free standing droplet whereas the latter was grown under controlled diffusion conditions from a pre-patterned Ge/Au film. Moreover, the SEM image in Fig. 5(f) demonstrates that while the nanowire placement is partially controlled by the pattern, the nanowire lengths vary from 2 μm to 50 μm. Length control remains a challenge and future studies will focus on ability to use micro and nano scale fluidic flows and agglomeration waves to control nanowire growth.

In conclusion, we have demonstrated a completely new form of nanowire growth based on surface energy driven diffusion, which has significant advantages over earlier methods. It eliminates the need for gas and solvent phase processing since the growth precursors are contained within the film. Incorporation of additional material components into the film offers the possibility of tuning the growth temperature and nanowire growth rates. Patterning of the film generates surface agglomeration waves that may provide a route to controlled nanowire placement with controlled diameters and perhaps controlled lengths. This flexibility in combination with the extraordinary simple growth process suggests that agglomeration growth may find wide ranging applications in the areas of sensors, devices and interconnects.

ACKNOWLEDGMENT

We acknowledge the Science Foundation Ireland funded Principal Investigator Award (Grant No. 06/IN.1/I106) and the collaboration between Trinity College Dublin, University College Cork, and Intel (SFI Grant 03/CE3/M406)

Supporting Information Available:

Extensive figures and analytical characterization data are available free of charge via the Internet at http://pubs.acs.org.

Figure and figure captions

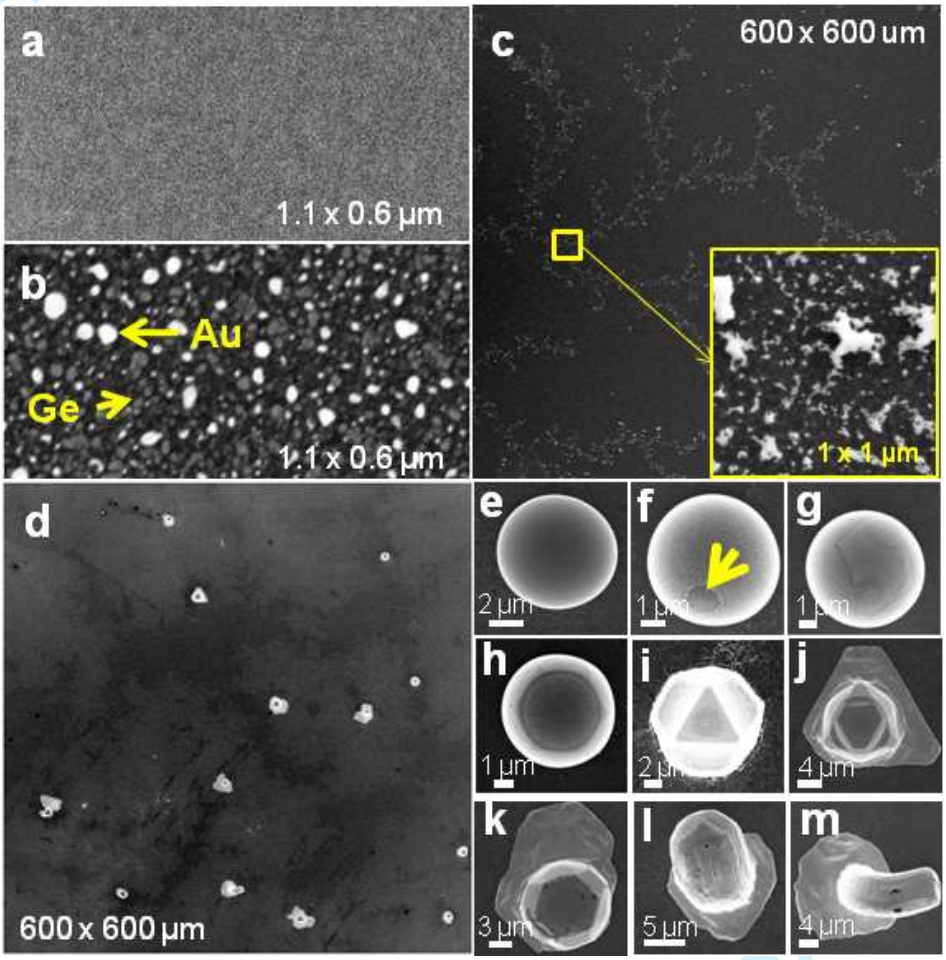

Figure 1. Au/Ge bilayer on Si(100) substrate comprised of: (a) Au 0 nm/Ge 10 nm layer, (b) Au 1 nm/Ge 10 nm bilayer (c) Au 5 nm/Ge 10 nm bilayer and (d) Au 10 nm/Ge 10 nm bilayer. These SEM images were taken at room temperature follows annealing at 400 °C for 12 hours. The SEM images in (e)-(m) are the enlarged features of eutectic balls in (d).

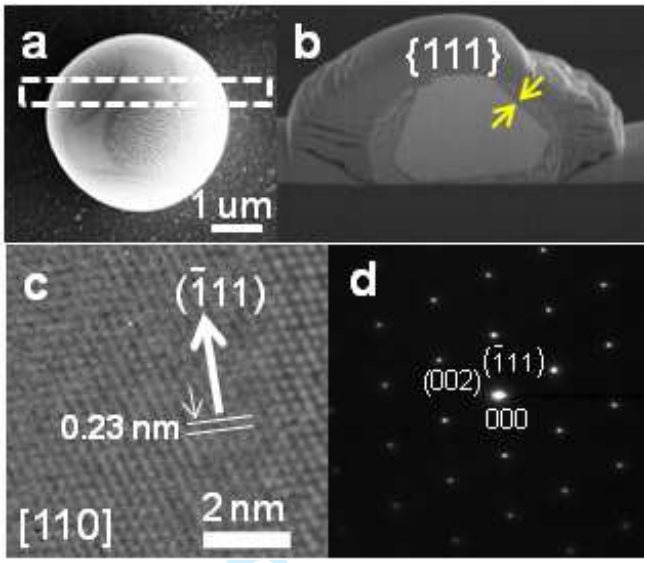

Figure 2. Detailed characterization of the eutectic droplet with Au supersaturation. (a) SEM image of droplet structure. White box indicates the outline of FIB cross section. (b) SEM image of cross section showing the presence of large Au crystal at center of the droplet. Yellow arrows indicate amorphous Ge layer surrounding Au crystal. (c) HRTEM image of Au crystal. (d) The electron diffraction pattern of corresponding area shows a [110] zone axis.

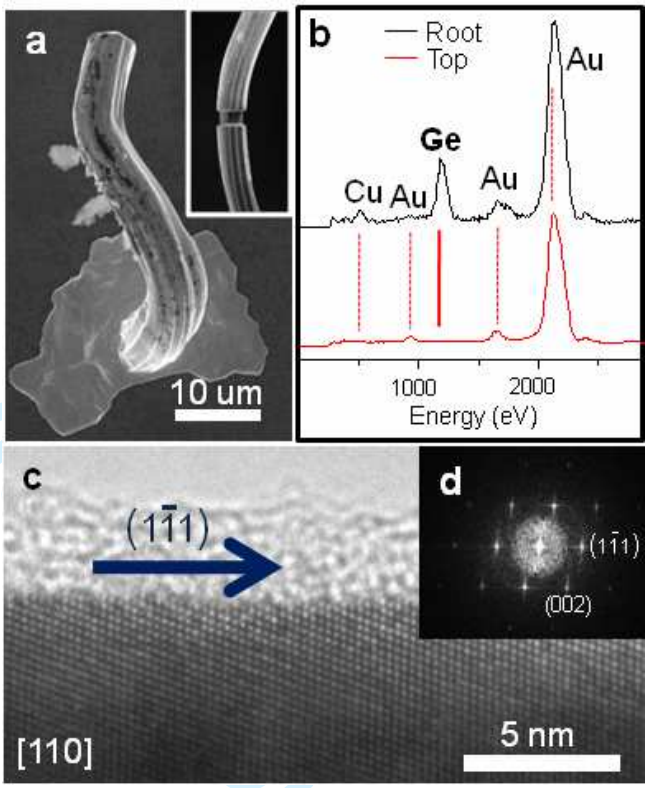

Figure 3. Au wire grown from the AuGe bilayer on the Si(100) surface. (a) SEM image of Au wire. Inset of a show the thinned wire for TEM analysis. (b) The EDX analysis of the Au wire indicate the presence of Ge in the root ball area which is not found in the spectrum associated with the top sections of the wire. (c) HRTEM image of Au crystal showing well resolved lattice planes. The amorphous surface layer is due to the FIB processing. (d) The FFT pattern of (c) indicating that the wire grows along the (1-11) direction (blue arrow in (c)).

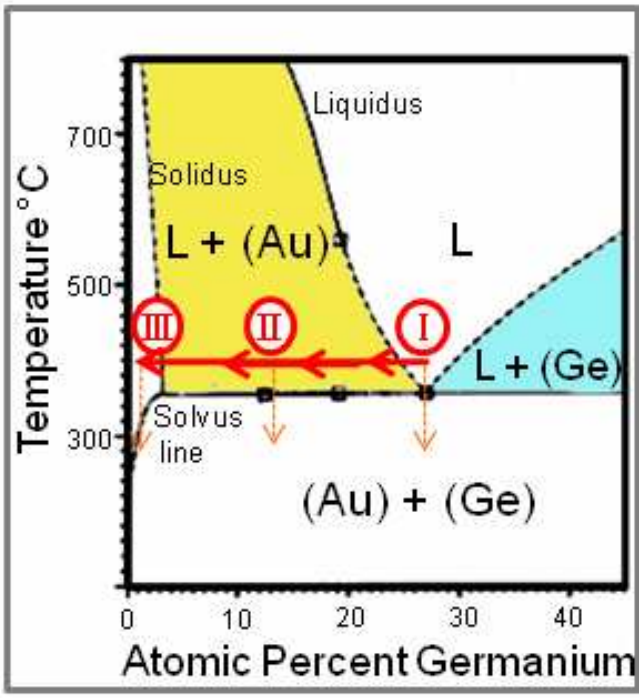

Figure 4. A section of binary phase diagram for an equilibrium Au-Ge alloy. The red line traces the Au enrichment and cooling paths associated with our growth mechanism.[19]

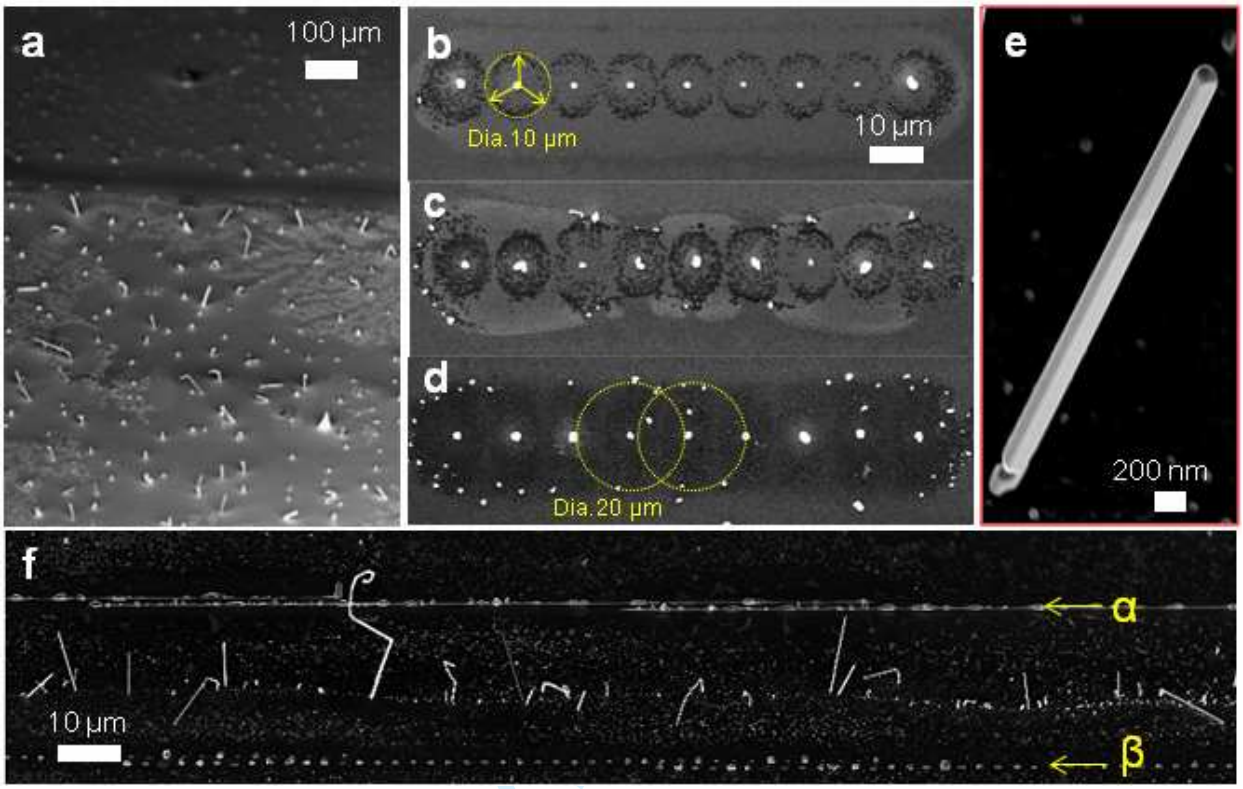

Figure 5. SEM images showing Au wires grown by controlling the atomic diffusion and aggregation dynamics. (a) Selectively grown Au wires on a 10 nm Au/10 nm Ge patterned region of a Si (100) substrate. (b) Circular wavefronts of materials spreads outwards from hole during the annealing process. (c) and (d) SEM images showing the interference of wavefronts. The yellow circles indicate the interference of the diffusion wavefronts. (f) Array of the single crystal Au wires positioned at the interference positions of α and β hole array. (e) Enlarged SEM image of one Au wire in (f)

(1) Wagner, R. S.; Ellis, W. C. *Appl. Phys. Lett.* **1964**, *4*, 89-90.
(2) Morales, A. M.; Lieber, C. M. *Science* **1998**, *279*, 208-211.
(3) Hochbaum, A. I.; Fan, R.; He, R. R.; Yang, P. D. *Nano Lett.* **2005**, *5*, 457-460.
(4) Fan, H. J.; Werner, P.; Zacharias, M. *Small* **2006**, *2*, 700-717.
(5) Wang, D.; Dai, H. *Appl. Phys. A* **2006**, *85*, 217-225.
(6) Shpyrko, O. G.; Streitel, R.; Balagurusamy, V. S. K.; Grigoriev, A. Y.; Deutsch, M.; Ocko, B. M.; Meron, M.; Lin, B.; Pershan, P. S. *Science* **2006**, *313*, 77-80.
(7) Adhikari, H.; Marshall, A. F.; Goldthorpe, I. A.; Chidsey, C. E. D.; McIntyre, P. C. *ACS Nano* **2007**, *1*, 415-422.
(8) Wang, D. W.; Tu, R.; Zhang, L.; Dai, H. J. *Angew. Chem.-Int. Edit.* **2005**, *44*, 2925-2929.
(9) Holmberg, V. C.; Panthani, M. G.; Korgel, B. A. *Science* **2009**, *326*, 405-407.
(10) Hannon, J. B.; Kodambaka, S.; Ross, F. M.; Tromp, R. M. *Nature* **2006**, *440*, 69-71.
(11) Chueh, Y.-L.; Boswell, C. N.; Yuan, C.-W.; Shin, S. J.; Takei, K.; Ho, J. C.; Ko, H.; Fan, Z.; Haller, E. E.; Chrzan, D. C.; Javey, A. *Nano Lett.* **2010**, *10*, 393-397.
(12) Law, M.; Goldberger, J.; Yang, P. *Annu. Rev. Mater. Res.* **2004**, *34*, 83-122.
(13) Sutter, P. W.; Sutter, E. A. *Nat Mater* **2007**, *6*, 363-366.
(14) Kodambaka, S.; Tersoff, J.; Reuter, M. C.; Ross, F. M. *Science* **2007**, *316*, 729-732.
(15) Wu, Y.; Cui, Y.; Huynh, L.; Barrelet, C. J.; Bell, D. C.; Lieber, C. M. *Nano Lett.* **2004**, *4*, 433-436.
(16) Eswaramoorthy, S. K.; Howe, J. M.; Muralidharan, G. *Science* **2007**, *318*, 1437-1440.
(17) Hu, S.; Leu, P. W.; Marshall, A. F.; McIntyre, P. C. *Nat. Nanotechnol.* **2009**, *4*, 649-653.
(18) Chen, Z. W.; Lai, J. K. L.; Shek, C. H.; Chen, H. D. *Appl. Surf. Sci.* **2005**, *250*, 3-8.
(19) Elliott, R.; Shunk, F. *J. Phase Equilib.* **1980**, *1*, 51-54.
(20) Konno, T. J.; Sinclair, R. *Mater. Sci. Eng., A* **1994**, *179-180*, 426-432.
(21) Herd, S. R.; Chaudhari, P.; Brodsky, M. H. *J. Non-Cryst. Solids* **1972**, *7*, 309-327.
(22) Sa, I.; Lee, B.-M.; Kim, C.-J.; Jo, M.-H.; Lee, B.-J. *Calphad* **2008**, *32*, 669-674.
(23) Witten, T. A.; Sander, L. M. *Phys. Rev. Lett.* **1981**, *47*, 1400-1403.
(24) Hou, J.-g.; Wu, Z.-q. *Phys. Rev. B* **1989**, *40*, 1008.
(25) Eftekhari, A. *Appl. Surf. Sci.* **2004**, *227*, 331-340.
(26) Enculescu, M.; Enculescu, I.; Topa, V. *J. Optoelectron. Adv. M.* **2006**, *8*, 1230-1233.
(27) Chidambaram, V.; Hald, J.; Hattel, J. *J. Alloys Compd.*, *490*, 170-179.
(28) Cleveland, C. L.; Landman, U.; Schaaff, T. G.; Shafigullin, M. N.; Stephens, P. W.; Whetten, R. L. *Phys. Rev. Lett.* **1997**, *79*, 1873-1876.
(29) Díaz, M.; et al. *Nanotechnology* **2003**, *14*, 113-116.
(30) Prabhakaran, K.; Maeda, F.; Watanabe, Y.; Ogino, T. In *1st Joint Conference on Silicon Epitaxy and Heterostructures (UC-Si)*; Elsevier Science Sa: Zao, Japan, 1999, p 289-292.
(31) Bracht, H.; Stolwijk, N. A.; Mehrer, H. *Phys. Rev. B* **1991**, *43*, 14465-14477.
(32) Wu, T. H.; Kuo, P. C.; Ou, S. L.; Chen, J. P.; Yen, P. F.; Jeng, T. R.; Wu, C. Y.; Huang, D. R. *Appl. Phys. Lett.* **2008**, *92*, 011126.
(33) Werner, M.; Mehrer, H.; Hochheimer, H. D. *Phys. Rev. B* **1985**, *32*, 3930.
(34) Nix, F. C.; MacNair, D. *Phys. Rev.* **1941**, *60*, 597.
(35) Kagaya, H.-M.; Soma, T. *Solid State Commun.* **1993**, *85*, 617-621.
(36) Acosta, R. E.; Johnson, W. A.; Berry, B. S.; Pritchet, W. C. *Microelectron. Eng.* **1992**, *17*, 189-192.
(37) Diao, J.; Gall, K.; Dunn, M. L. *Nat Mater* **2003**, *2*, 656-660.
(38) Shim, W.; Ham, J.; Lee, K. I.; Jeung, W. Y.; Johnson, M.; Lee, W. *Nano Lett.* **2009**, *9*, 18-22.
(39) Tu, K. N. *Phys. Rev. B* **1994**, *49*, 2030-2034.
(40) Lee, B. Z.; Lee, D. N. *Acta Mater.* **1998**, *46*, 3701-3714.
(41) Fisher, R. M.; Darken, L. S.; Carroll, K. G. *Acta Metall.* **1954**, *2*, 368-&.
(42) Tu, K. N. *Phys. Rev. B* **1994**, *49*, 2030.
(43) Floro, J. A.; Chason, E.; Cammarata, R. C.; Srolovitz, D. J. *MRS Bull.* **2002**, *27*, 19-25.
(44) Olesinski, R.; Abbaschian, G. *J. Phase Equilib.* **1986**, *7*, 28-35.
(45) Tadepalli, R.; Thompson, C. V. *Appl. Phys. Lett.* **2007**, *90*, 3.
(46) Danielson, D. T.; Sparacin, D. K.; Michel, J.; Kimerling, L. C. *J. Appl. Phys.* **2006**, *100*, 083507.
(47) Srolovitz, D. J.; Goldiner, M. G. *JOM-J. Miner. Met. Mater. Soc.* **1995**, *47*, 31-36.

Table of Contents Graphic